Solar Energy Advances 4 (2024) 100067

Contents lists available at ScienceDirect

Solar Energy Advances

journal homepage: www.elsevier.com/locate/seja

Design and modeling of PV-integrated Double Skin Facades and application to retrofit buildings☆

Somil Yadav [a], Caroline-Hachem Vermette [b,*], Md.Nadim Heyat Jilani [b], Gilles Desthieux [c]

[a] Department of Civil and Infrastructure Engineering, Indian Institute of Technology, Dharwad, India
[b] Department of Building, Civil and Environmental Engineering, Concordia University, Montreal, Canada
[c] Haute École du Paysage d'Ingénierie et d'Architecture de Genève (HEPIA), University of Applied Sciences and Arts Western Switzerland (HES-SO), Switzerland

ARTICLE INFO

Keywords:
Double skin façade
PV-DSF systems
Coloured PV modules
Energy balance approach
Early design stage
Mathematical model

ABSTRACT

Double Skin Façade (DSF) system comprises two glazing layers with a ventilated cavity. Integrating photovoltaic (PV) modules within the outer layer of DSFs offers an efficient method for electricity generation. Current tools for modeling and analyzing DSF systems are complex and resource-intensive, lacking the capability to evaluate the performance of innovative PV-DSF systems during the early design stage. This study develops a mathematical model to evaluate the electrical and thermal performance of PV-DSF systems, considering architectural design elements such as PV color and relative orientation. Based on an energy balance approach, the model is particularly suited for designing PV-DSF systems in heritage buildings, which often have color and relative orientation constraints. The model is applied to assess the performance of PV-DSF systems with conventional clear glass PV and colored front glass PV modules under the climatic conditions of Montreal, Canada. Results indicated that conventional clear glass PV module exhibit higher PV cell temperature than colored PV modules due to greater transmissivity, with peak temperature differences at noon of 5.5 °C, 6.2 °C, and 6.5 °C for orange, blue, and gray PV modules, respectively. On the contrary, the influence of PV's color front glass on room air temperature is non-significant. Furthermore, the optimal orientation for maximum energy yield is not always south-facing; it depends on the hourly distribution of the beam, diffuse solar irradiation, and ambient air temperature. For Montreal, west-facing DSFs produce more electrical and thermal energy on a summer design day because the hourly distribution of beam radiation is skewed towards afternoon hours.

1. Introduction

Double-skin facades (DSFs) are an architectural concept that integrates two skins of glazing or other translucent materials with a cavity in between, which could be utilized for natural or artificial ventilation. Double Skin Façade is a time-tested technology for enhancing building energy efficiency and indoor environmental quality [1]. Combining solar photovoltaic (PV) elements with the DSF concept offers additional advantages of renewable electricity generation. In the field of building construction technologies, attempts have always been made to enhance the performance of building facades, which serve as the principal interface between the internal and external environments. Considering prevailing environmental conditions (solar radiation, ambient air temperature, and humidity) along with the desired comfortable internal environment for occupants is a must while deciding on a building's façade [2–4]. Considering the above-listed factors is even more crucial in the case of DSF design since DSF can alter solar radiation, thermal amplitudes, and the ability to employ passive and active technologies. Several parameters need to be considered during the modeling and design of ventilated PV-DSF systems, including the cavity depth and height [5], the properties of the outer and inner skin [6], orientation and tilt angles of PV panels [7], and the structure of the DSF system [8]. These parameters play a key role in optimizing the performance and functionality of ventilated PV-DSF systems.

2. Literature review

Several researchers have analyzed the performance of Double Skin Façade (DSF) systems using both analytical and experimental

☆ This paper was submitted to and presented at EuroSun 2024 – the ISES and IEA SHC International Conference on Sustainable and Solar Energy for Buildings and Industry.

* Corresponding author.
E-mail address: caroline.hachemvermette@concordia.ca (C.-H. Vermette).

https://doi.org/10.1016/j.seja.2024.100067
Received 10 July 2024; Received in revised form 23 August 2024; Accepted 3 September 2024
Available online 8 September 2024

Nomenclature

Acronyms

BIPV	building integrated photovoltaics
DSF	double skin facade
LTG	low-iron tempered glass
PV	photovoltaic
PV/T	photovoltaic thermal
STC	standard test condition

Roman letters

A	area (m^2)
b	width (m)
C	specific heat (J kg^{-1} °C)
D	thickness/depth (m)
E	electrical energy (kWh)
h	convective heat transfer coefficient (W m^{-2} °C $^{-1}$)
$I_{glob,inc}$	global/total solar irradiation (W m^{-2})
K	thermal conductivity (W m^{-1} °C $^{-1}$)
L	length/height (m)
M	mass (kg)
$\dot{m}$	mass flow rate (kg s^{-1})
N	number of air changes per hour
Q	thermal energy (kW h)
R	tilt factor for beam radiation (View factor in case of diffuse and reflected radiation)
T	temperature (°C)
$\overline{T}$	average temperature over cavity length (°C)
U	overall heat transfer coefficients (W m^{-2} °C $^{-1}$)
V	volume of room (m^{-3})

Greek letters

α	absorptivity
β	inclination angle of PV
β_c	packing factor of PV
β_{ref}	temperature coefficient of PV
τ	transmissivity
η	PV module's electrical efficiency
ρ_f	density of air (kg/m^3)
ρ_g	ground surface albedo

Subscript

am	ambient
bs	back-sheet
beam	beam radiation
c	PV cell
cv	cavity
diffuse	diffuse radiation
f	air
fg	cavity behind glass facade
fpv	cavity behind PV facade
g	glass façade
glob	global or total
i	interior glass facade
in	cavity inlet
inc	inclined or tilted surface
inst	instantaneous
out	cavity outlet
pv	PV facade
r	room
ref	STC reference
td	tedlar
tg	top glass of PV
w	wall
refl	ground reflected radiation

approaches across various climatic conditions. For instance, Torres et al. [9] simulated the impact of DSF cavity widths and external openings on the annual cooling and heating loads of an office building in Mediterranean climates. Their findings indicated that wider cavities reduce the cooling load more effectively than narrower ones, while increasing cavity openings further enhances this effect. However, larger cavities and openings also lead to higher heating loads. The variation in cavity dimensions can significantly alter the thermal dynamics within the cavity, potentially affecting the performance of integrated Photovoltaic (PV) elements. Ziasistani et al. [10] explored the impact of orientation on the energy performance of DSF systems across six different climatic conditions, finding that energy demand is highest when the DSF faces west, while energy generation peaks with a south-facing DSF. Other studies, such as those by Marinosci et al. [11] and Fantucci et al. [12], experimentally examined opaque DSF systems for Italian climatic conditions, focusing on the influence of incident solar radiation on facade temperatures. Mateus et al. [13] validated a dynamic simulation model for a glazed DSF system in Lisbon, while Qahtan et al. [14] investigated the performance of a glazed DSF in Malaysia's tropical climate, concluding that direct solar radiation significantly impacts indoor air temperatures, necessitating improved solar shading technologies. While these studies provide valuable insights, a key limitation in the existing literature is the tendency to evaluate DSF systems without considering them integral parts of the building. This approach overlooks the DSF's impact on the indoor thermal environment, a critical factor for comprehensive analysis. Although Computational Fluid Dynamics (CFD) [15] techniques are recognized as effective tools for analyzing the thermo-fluid dynamic behavior of DSF systems, their integration with building energy simulation (ES) models [16] offers more accurate results. However, it demands significant computational resources and is not well-suited for early design stages [17].

In heritage buildings, retrofitting facades with PV-DSF systems offers a promising avenue for converting conventional facades into energy generators. However, preserving architectural features, including the color and orientation of facades, is paramount in such projects. This necessitates using colored PV modules, which can be achieved by adding color to solar cells, encapsulants, or cover glass using techniques like dot printing or sputter coating. However, adding color to PV modules alters their transmissivity and standard electrical efficiency. Studies [18] have shown that gray-colored PV modules experience a 7 – 10 % reduction in performance, while red-colored modules see a 16 % decrease in performance compared to conventional PV modules. Similarly, Jolissaint et al. [19] concluded that green, blue, gray, and gold-colored PV modules experienced performance reductions of 16 %, 20 %, 24 %, and 24 %, respectively, compared to conventional PV modules due to transmission losses. These findings underscore the necessity of accounting for the color of PV modules in the mathematical modeling of PV-DSF systems.

A thorough review of existing research on ventilated PV Double Skin Façade (DSF) systems in the open literature highlights two key gaps: (1) the absence of an early-stage design model to evaluate the performance of DSF systems and their impact on indoor air temperature, and (2) a lack of models that consider the specific architectural constraints of heritage buildings, such as color preservation and orientation. These limitations restrict the comprehensive evaluation of innovative PV-DSF systems, particularly in retrofitting projects related to heritage buildings where preserving historical features is critical. The present study addresses these gaps by developing a novel mathematical model designed to evaluate the electrical and thermal performance of PV-DSF systems

while considering architectural design elements such as PV module color and relative orientation. Unlike existing models, this approach integrates the DSF as an essential part of the building, allowing for a comprehensive analysis of its impact on indoor air temperature. The model is based on an energy balance method, offering a streamlined yet robust tool that is particularly suited for the preliminary design stages. Its applicability to heritage buildings, where color and orientation constraints are paramount, represents a significant advancement in the field, facilitating the retrofitting of such structures with energy-efficient technologies.

3. Problem overview

This study explores the impact of colored PV modules and their orientation on the electrical and thermal performance of a ventilated Double Skin Facade (DSF) system. The exterior facade of the DSF features an opaque PV segment, where various colored PV modules, namely grey, blue, and orange, are integrated alongside a transparent glass segment. The coloration of the PV modules is achieved by applying a sputter coating layer on the inner surface of low-iron tempered glass. The structure of the colored photovoltaic module and the physical principle of sputter coating are depicted in Fig. 1a. The glass color variation is controlled by adjusting the thickness of the sputter coating layer, which reflects specific visible wavelengths. The properties of color PV modules are presented in Table 1a below [20]. The interior facade of the DSF is entirely made of glass, creating a cavity between the interior and exterior facades through which airflow is provided (Fig. 1b). The cavity inlet connects to the ambient outdoor air, while the outlet links to the indoor air. This airflow helps reduce the PV cell temperature, enhancing efficiency and providing warm air for space conditioning. A small exhaust fan is assumed to drive the airflow within the cavity. Montreal, Canada (latitude 52° N), serves as a pilot study location. For the performance evaluation, the room volume is considered to be 27 m^3, with an infiltration rate (air leakage loss) of 0.2 air changes per hour. A packing factor (β_c) of 0.8 was assumed for the photovoltaic (PV) segment, accompanied by a K_L value set to 0.5, indicating an equal distribution of PV and glass components within the exterior facade. The transmissivity (τ_g) of the exterior glass facade was established at 0.5, and the airflow rate ($\dot{m}_f$) within the cavity was maintained at a fixed value of 0.025 kg s^{-1}. Further, the design parameters of the DSF system are detailed in Table 1b, and the assumptions for the mathematical model are outlined in Section 4: Mathematical Modeling.

4. Mathematical formulation

The proposed mathematical model for evaluating the performance of the ventilated PV double-skin façade (DSF) system adopts an energy balance approach. The model is developed under the following assumptions:

(i) Heat transfer through the DSF system is considered to be one-dimensional.
(ii) The system operates in a quasi-steady state.
(iii) The thermophysical properties of materials remain constant within the system's operational temperature range.
(iv) The airflow within the cavity is in laminar condition, i.e., R_e (Reynold's number) $< 4 \times 10^5$.
(v) Internal heat gains from occupants, lighting, and appliances are neglected.

The energy equilibrium equations for different PV DSF system components shown in Fig. 1c are written below.

4.1. Opaque color PV segment of double skin façade

4.1.1. Front side of opaque photovoltaic exterior facade

The solar energy incident on both the PV area (packing area) and the Tedlar area (non-packing area) equals the sum of the electrical energy generated and the heat transferred from the PV module to the surrounding air and the opaque back sheet. This energy balance is mathematically expressed as follows.

$$\tau_{tg}\{\alpha_c\beta_c + (1-\beta_c)\alpha_{td}\}I_{glob,\,inc}\,bdx = U_{c,am}(T_c - T_{am})\,bdx + U_{c,bs}(T_c - T_{bs}) + \eta_{ref}\beta_c I_{glob,\,inc}\,bdx \quad (1a)$$

To account for the color in the PV module, the transmissivity (τ_{tg})

Table 1a
Properties of conventional and color PV modules [20].

PV Module		Transmissivity,τ_{tg} (%)	STC efficiency (%)
Conventional (clear front glass cover)		91.51	17.95
Orange		79.48	16.38
Blue		77.63	16.61
Gray		76.5	16.06

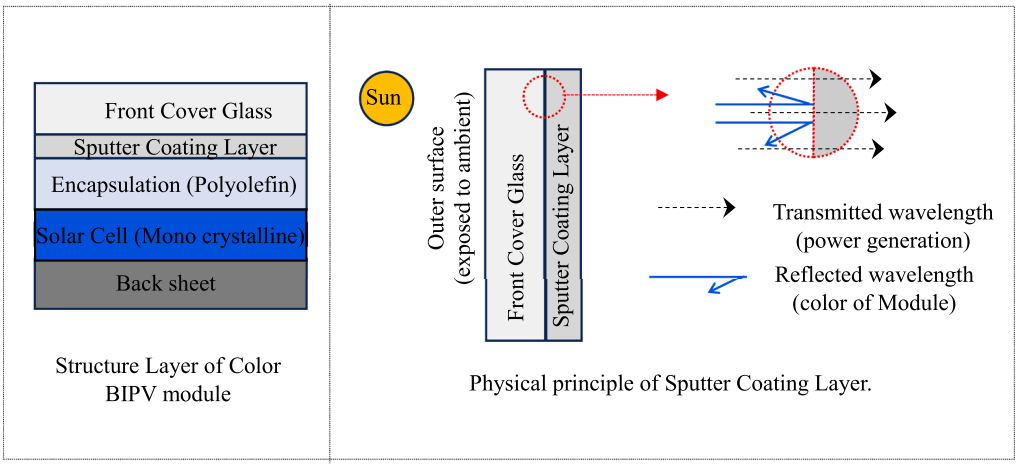

Fig. 1a. Structural layer of color PV module and physical principle of Sputter Coating Layer.

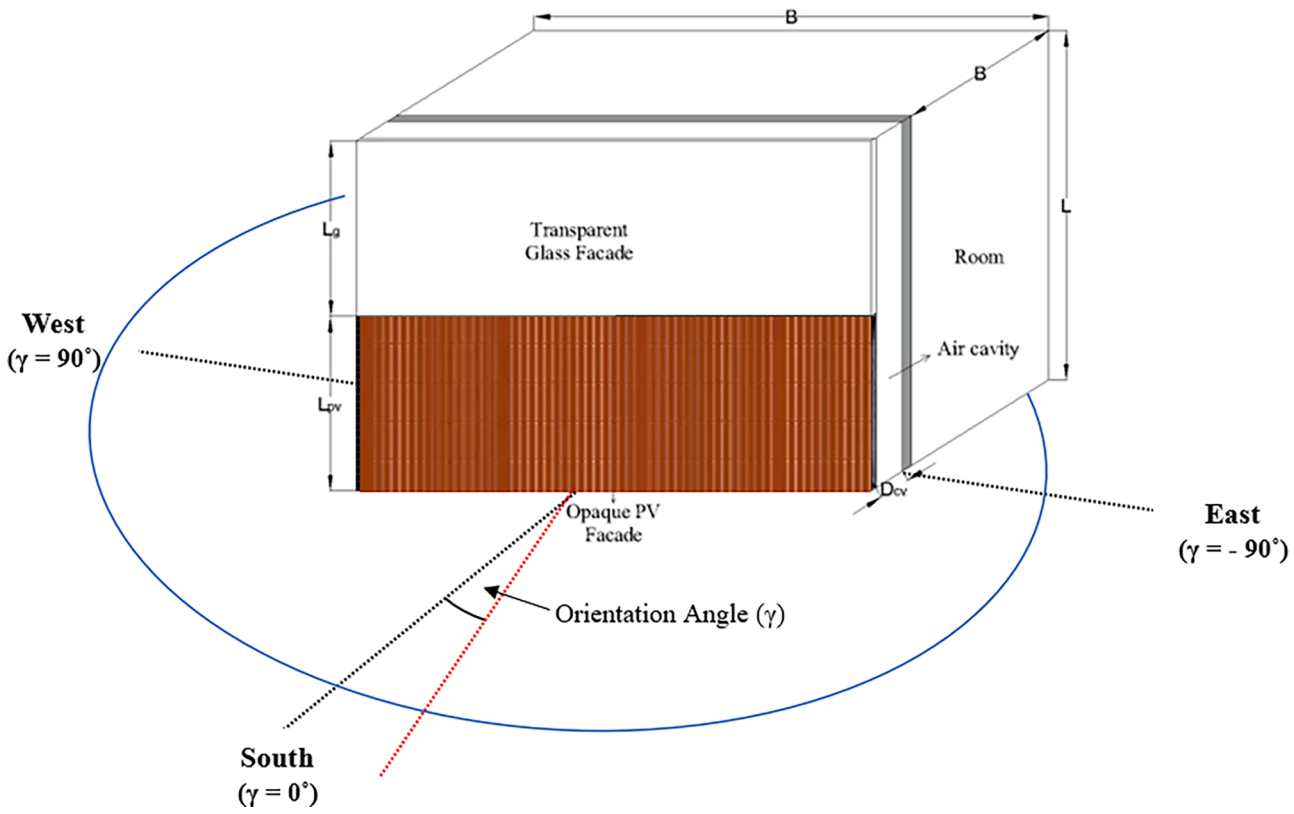

Fig. 1b. Isometric view of a typical box type double skin façade system with a ventilated air cavity.

Table 1b
Design parameters of PV DSF systems [21].

A_{pv}	2.25 m^{-2}	K_{bs}	0. 033 W m^{-1} °C^{-1}	$U_{f,r}$	2.0 W m^{-2} °C^{-1}
A_g	2.25 m^{-2}	K_g	1.0 W m^{-1} °C^{-1}	$U_{r,am}$	1.0 W m^{-2} °C^{-1}
b	1.5 m	K_i	0.35 Wm^{-1} °C^{-1}	V	27 m^{-3}
C_f	1005 J $Kg^{-1}C^{-1}$	K_{tg}	1.0 W m^{-1} °C^{-1}	α_c	0.90
D_{cv}	0.15 m	L	3.0 m	α_g	0.50
D_{bs}	0.005 m	L_g	1.5 m	α_{td}	0.50
D_g	0.003 m	L_{pv}	1.5 m	β_{ref}	0.0045
D_i	0.05 m	M	32.40 kg	β_c	0.80
D_{tg}	0.003 m	$\dot{m}_f$	0.025 kg s^{-1}	ρ_f	1.77 kg m^{-3}
h_{am}	9.50 W m^{-2} °C^{-1}	N	0.2 per hour	τ_g	0. 50
$h_{bs,f}$	1.9 W m^{-2} °C^{-1}	$U_{c,am}$	9.23 W m^{-2} °C^{-1}	τ_{tg}	0.91
$h_{g,f}$	1.9 W m^{-2} °C^{-1}	$U_{c,bs}$	6.6 W m^{-2} °C^{-1}	η_{ref}	0.18
h_r	2.8 W m^{-2} °C^{-1}	$U_{g,am}$	9.23 W m^{-2} °C^{-1}		

values of the front glass cover and STC efficiency (η_{ref}) of the PV module are updated as per Table 1a in the above equation. This equation is further rearranged to derive an expression for the PV cell temperature, as shown below.

$$T_c = \frac{\alpha_{eff} I_{glob,\,inc} + U_{c,am} T_{am} + U_{c,bs} T_{bs}}{U_{c,am} + U_{c,bs}} \tag{1b}$$

Here,'$U_{c,am}$' and '$U_{c,bs}$' represent the overall heat transfer coefficients from the PV module to the ambient and the back sheet, respectively. These coefficients are defined as follows.

$$U_{c,am} = \left[\frac{D_{tg}}{K_{tg}} + \frac{1}{h_{am}}\right]^{-1}; U_{c,bs} = \left[\frac{D_{bs}}{K_{bs}}\right]^{-1}; \alpha_{eff} = \tau_{tg}\{\alpha_c\beta_c + (1-\beta_c)\alpha_{td}\} - \eta_{ref}\beta_c \tag{1c}$$

Additionally, to account for the impact of the DSF's orientation in the mathematical model, the value of solar irradiation ($I_{glob,inc}$) in Eq. (1) and the subsequent equations should be updated according to the Liu and

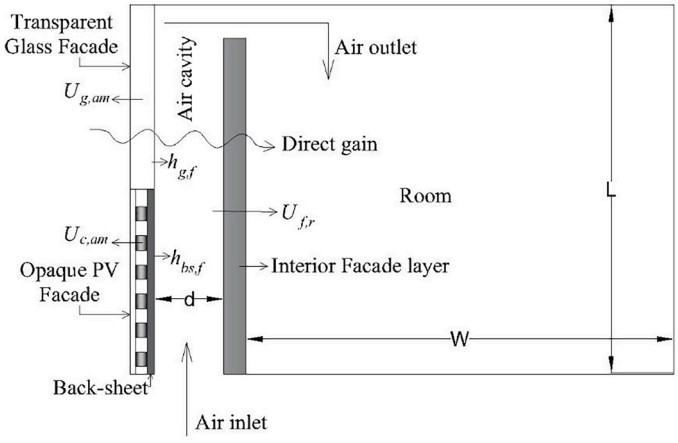

Fig. 1c. Cross-sectional view of a typical box type double skin façade system with a ventilated air cavity [21].

Jordan model [22], as detailed below. According to this model, the total irradiation comprises beam, diffuse, and ground-reflected components, as shown by Eq. (2) below.

$$I_{glob,inc} = I_{beam,inc} + I_{diffuse,inc} + I_{refl,inc} \tag{2}$$

The beam radiation is a component of the total radiation directly received by a surface from the sun. It is calculated using the global (I_{glob}) and diffuse ($I_{diffuse}$) solar irradiation received on a horizontal surface. The mathematical expression for this is provided below.

$$I_{beam,\,inc} = R_{beam}\left(I_{glob} - I_{diffuse}\right) \tag{3a}$$

here, the tilt factor, represented by (R_{beam}), accounts for the varying inclinations and orientations of the surface under consideration. It is

defined as the ratio of beam radiation on a tilted surface to that on a horizontal surface and is mathematically expressed as follows.

$$R_{beam} = \frac{\cos\theta_i}{\cos\theta_z} = \frac{C_1\cos\delta\cos\omega + C_2 + C_3\sin\delta}{\sin\delta\sin\phi + \cos\delta\cos\phi\cos\omega} \tag{3b}$$

C_1, C_2, *and* C_3 are coefficients given by Eq. (3c).

$$C_1 = \cos\phi\cos\beta + \sin\phi\sin\beta\cos\gamma\ ;\ C_2 = \cos\delta\sin\omega\sin\beta\sin\gamma\ ;\ C_3 = \sin\phi\cos\beta - \cos\phi\sin\beta\cos\gamma \tag{3c}$$

where, 'θ_i' is the incident angle of irradiation, 'θ_z' is the zenith angle, 'ϕ' is the location's latitude, 'β' is the tilt angle, 'ω' is the hour angle, 'δ' is the declination angle, and 'γ' is the azimuth angle (orientation) of the tilted surface. $\gamma = 0^\circ$ indicates south-facing DSF, and $\gamma = +90$ and -90° correspond west and east-facing DSF, respectively.

The second component of total irradiation is diffuse irradiation, which is determined for an inclined surface as follows.

$$I_{diffuse,\,inc} = R_{diffuse} \times I_{diffuse} \tag{4a}$$

The diffuse view factor to the sky ($R_{diffuse}$) can be determined using Eq. (4b), as shown below.

$$R_{diffuse} = \frac{1+\cos\beta}{2} \tag{4b}$$

Finally, the ground-reflected irradiation on the tilted surface is calculated as given below.

$$I_{refl,\,inc} = \rho_g\left(I_{beam} + I_{diffuse}\right)R_{refl} \tag{5a}$$

where, 'R_{refl}' is the view factor to the ground and can be obtained by Eq. (5b).

$$R_{refl} = \frac{1-\cos\beta}{2} \tag{5b}$$

The value of 'ρ_g' ranges from 0.2 to 0.7, depending on the surrounding area [23]. For typical ground surfaces, a value of 0.2 can be used.

4.1.2. Rear side of opaque photovoltaic exterior façade

The energy received by the rear side (back sheet) equals the energy transferred to the air flowing through the cavity via convection.

$$U_{c,bs}(T_c - T_{bs})\,bdx = h_{bs,f}\left(T_{bs} - T_{fpv}\right)bdx \tag{6a}$$

where, '$h_{bs,f}$' denotes the convective heat transfer coefficient for air moving through the cavity, and it is a function of Reynolds' 'Re' and Prandtl's 'Pr' numbers, expressed below [24].

$$h_{bs,f} = \frac{K}{L}(0.664)\mathrm{Re}^{0.5}\mathrm{Pr}^{0.33} \tag{6b}$$

Substituting the expression of 'T_c' from Eq. (1b) into Eq. (6a), the back-sheet temperature 'T_{bs}' is expressed as follows.

$$T_{bs} = \frac{h_{p1}\alpha_{eff}I_{glob,inc} + U_{tT}T_{am} + h_{bs,f}\overline{T}_{fpv}}{U_{tT} + h_{bs,f}} \tag{6c}$$

where, 'h_{p1}' is the penalty factor due to the presence of PV cell material, Tedlar, and back-sheet; it is defined below.

$$h_{p1} = \frac{U_{c,bs}}{U_{c,am} + U_{c,bs}};\ U_{tT} = \frac{U_{c,bs}U_{c,am}}{U_{c,am} + U_{c,bs}} \tag{6d}$$

4.1.3. Airflow in the PV segment's rear cavity of the DSF

$$h_{bs,f}\left(T_{bs} - T_{fpv}\right)bdx = \dot{m}_f C_f\frac{dT_{fpv}}{dx}dx + U_{f,r}\left(T_{fpv} - T_r\right)bdx \tag{7a}$$

The energy balance described above is used to calculate the average air temperature along the length of the PV cavity ($\overline{T}_{fpv}$) and the air temperature at the outlet ($T_{fpv,out}$) based on the specified boundary condition at the inlet, i.e., at $x = 0$, $T_{fpv} = T_{fpv,in}$. The resulting expressions for $\overline{T}_{fpv}$ and $T_{fpv,out}$ are presented below, and a detailed solution is provided in Appendix A.

$$T_{fpv,out} = T_{fpv}(x = L_{pv}) = \left(\frac{U_{f,r}T_r + U_{ta}T_{am} + h_{p2}h_{p1}\alpha_{eff}I_{glob,inc}}{U_L}\right)\left(1 - e^{-pL_{pv}}\right) + T_{fpv,in}e^{-pL_{pv}} \tag{7b}$$

$$\overline{T}_{fpv} = \left(\frac{U_{f,r}T_r + U_{ta}T_{am} + h_{p2}h_{p1}\alpha_{eff}I_{glob,inc}}{U_L}\right)\left(1 - \frac{1 - e^{-pL_{pv}}}{pL_{pv}}\right) + T_{fpv,in}\left(\frac{1 - e^{-pL_{pv}}}{pL_{pv}}\right) \tag{7c}$$

4.2. Transparent glass segment of double skin façade

4.2.1. Exterior glass façade layer

$$\alpha_g I_{glob,inc}\,bdx = U_{g,am}\left(T_g - T_{am}\right)bdx + h_{g,f}\left(T_g - \overline{T}_{fg}\right)bdx \tag{8a}$$

The above equation can be rearranged to express the glass façade temperature as given below.

$$T_g = \frac{\alpha_g I_{glob,inc} + T_{am}U_{g,am} + T_{fg}h_{g,f}}{U_{g,am} + U_{g,f}} \tag{8b}$$

where, $U_{g,am} = \left[\frac{D_g}{K_g} + \frac{1}{h_{am}}\right]^{-1}$ is the overall heat transfer from glass to ambient, and '$h_{g,f}$' is the convective heat transfer from glass to the air flowing through the cavity.

4.2.2. Airflow in the glass segment's rear cavity of the DSF

$$h_{g,f}\left(T_g - T_{fg}\right)bdx = \dot{m}_f C_f\frac{dT_{fg}}{dx}dx + U_{f,r}\left(T_{fg} - T_r\right)bdx \tag{9a}$$

The equation above can be solved analogously to Eq. (7), incorporating the boundary conditions as, at $x = (L - L_{pv})$, $T_{fg} = T_{fpv,out}$. i.e., air temperature at the inlet of the glass façade equals that at the outlet of the PV facade. The resulting expressions are provided below.

$$\overline{T}_{fg} = \left(\frac{h_{p1g}\alpha_g I_{glob,inc} + U_{f,r}T_r + U_{tag}T_{am}}{U_{Lg}}\right)\left(1 - \frac{1 - e^{-p_g L_g}}{p_g L_g}\right) + T_{fpv,out}\left(\frac{1 - e^{-p_g L_g}}{p_g L_g}\right) \tag{9b}$$

$$T_{fg,out} = \left(\frac{h_{p1g}\alpha_g I_{glob,inc} + U_{f,r}T_r + U_{tag}T_{am}}{U_{Lg}}\right)\left(1 - e^{-p_g L_g}\right) + T_{fpv,out}e^{-p_g L_g} \tag{9c}$$

where

$$h_{p1g} = \frac{h_{g,f}}{h_{g,f} + U_{g,am}};\ U_{tag} = \frac{h_{g,f}U_{g,am}}{h_{g,f} + U_{g,am}};\ U_{Lg} = \left(U_{tag} + U_{g,am}\right);\ p_g = \frac{bU_{Lg}}{\dot{m}_f C_f} \tag{9d}$$

4.3. Room air

The variation in room air temperature correlates with several factors: direct thermal gain from the glass façade, indirect thermal gain from the backs of opaque photovoltaic (PV) and glass façade sections, thermal energy introduced by air flowing through the cavity, and thermal losses from the room to the surroundings through ventilation, infiltration, and wall conduction. This relationship can be mathematically expressed as follows:

$$U_{f,r}(\overline{T}_{fpv} - T_r)A_{pv} + \dot{m}_f C_f (T_{fpv,out} - T_r) + {\tau_g}^2 I_{glob,inc} A_g + U_{f,r}(\overline{T}_{fg} - T_r)A_g + \dot{m}_f C_f (T_{fg,out} - T_r) = M_f C_f \frac{dT_r}{dt} + 0.33NV(T_r - T_{am}) + U_{r,am}(T_r - T_{am})A_w \quad (10a)$$

The room energy balance equation can be rearranged in the following form, which can be solved for the given initial condition, i.e., at $t = 0,\ T_r = T_{r,initial}$.

$$\frac{dT_r}{dt} + aT_r = f(t) \quad (10b)$$

$$T_r = \frac{f(t)}{a}\left(1 - \frac{1 - e^{-at}}{at}\right) + T_{r,initial}\left(\frac{1 - e^{-at}}{at}\right) \quad (10c)$$

where,

$$a = \left(U_{f,r}A_{pv} + \dot{m}_f C_f + U_{f,r}A_g + \dot{m}_f C_f + 0.33NV + U_{r,am}A_w\right)$$
$$f(t) = \left(U_{f,r}A_{pv}\overline{T}_{fpv} + \dot{m}_f C_f T_{fpv,out} + \tau^2{}_g I_{glob,inc}A_g + U_{f,r}A_g\overline{T}_{fg} + \dot{m}_f C_f T_{fg,out} + 0.33NVT_{am} + U_{r,am}A_w T_{am}\right) \quad (10d)$$

Once the room air temperature under given initial conditions is determined using Eq. (10c), temperatures of the PV façade and glass façade can be calculated using Eq. (1b) and Eq. (8b). Subsequently, the instantaneous electrical efficiency of the PV module (η_{ie}) and electrical energy ($\dot{E}_{inst}$) can be evaluated as described below [25].

$$\eta_{inst} = \eta_{ref}\left[1 - \beta_{ref}\left(T_c - T_{ref}\right)\right] \quad (11)$$

$$\dot{E}_{inst} = \eta_{inst}\alpha_c\tau_{tg}\beta_c A_{pv} I_{glob,inc} \quad (12)$$

Further, the thermal energy delivered by the DSF system can be calculated as given below.

$$\dot{Q}_{inst} = \dot{m}_f C_f \left(T_{fg,out} - T_r\right) \quad (13)$$

5. Methodology

The mathematical model is implemented in MATLAB to comprehensively evaluate the performance of the ventilated PV Double Skin Façade (DSF) system. Environmental data, including ambient air temperature and global solar radiation, specific to winter and summer design days, were sourced from the EnergyPlus database [26]. Incident solar radiation on the vertical south face of the DSF and for other orientations was computed using the Liu and Jordan model [27]. The following steps were undertaken to analyze the electrical and thermal performance of the DSF and its effects on indoor conditions.

1. The room air temperature was determined using Eq. (10c) under specific initial conditions.
2. Average air temperatures over the length of the cavity and at the outlet were computed for both the PV ($T_{fpv,out}$, $\overline{T}_{fpv}$) and glass segments ($T_{fg,out}$, $\overline{T}_{fg}$) using Eq. (7) and Eq. (9), respectively.
3. The temperatures of the PV and glass segments of the exterior façade were derived using Eqs. (1b) and (8b), utilizing the computed cavity air temperatures.
4. Finally, the electrical and thermal outputs of the DSF system were quantified using Eq. (12) and Eq. (13), respectively.

6. Results and discussion

The present mathematical model is validated by comparing the results computed by the model with that of Tiwari et al. [28]. Tiwari et al. evaluated the performance of an unglazed hybrid PV/T air collector exposed to ambient conditions on both the front and rear sides. The present ventilated PV DSF can be treated equivalent to the PV/T air collector system by assuming that the average air temperature in the room integrated with the DSF matches the ambient air temperature. The same climatic data used by Tiwari et al. is utilized in the present mathematical model to evaluate air temperature within the air cavity. As shown in Fig. 2, the outlet air temperature predicted by the current model closely matches the temperature estimated by Tiwari et al. The correlation coefficient of 0.99 indicates a strong agreement between the two sets of results. Furthermore, the model is utilized to assess the performance of the ventilated DSF system in the climatic conditions of Montreal, Canada. For this analysis, the coldest sunny day of the year (January 18) is chosen as the winter design day, and the warmest sunny day (July 15) is selected as the summer design day for Montreal, Canada.

Figs. 3a and 3b depict the hourly variation of beam and diffuse radiation on a horizontal surface and the ambient air temperature for the

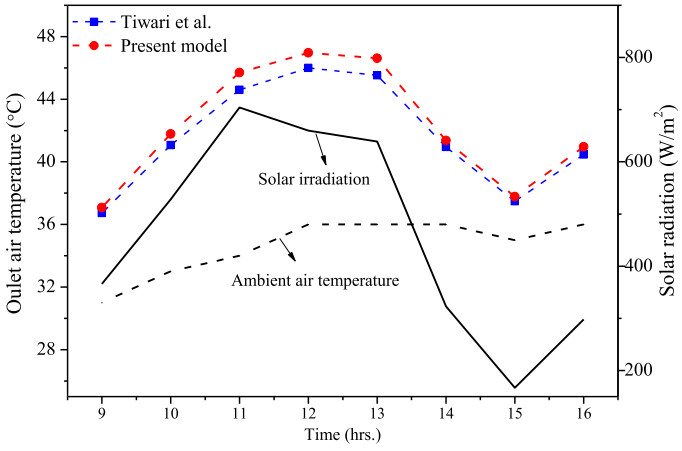

Fig. 2. Comparison of the outlet air temperature of PV/T air collector computed by the present model with Tiwari et al. [28].

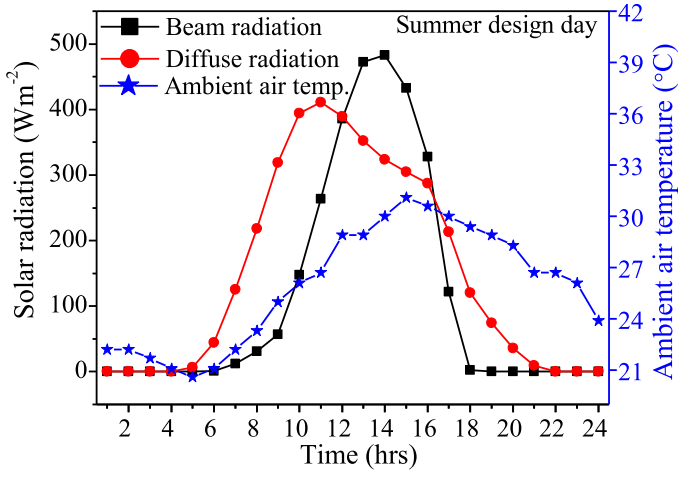

Fig. 3a. Hourly variation of the horizontal beam, diffuse solar irradiation, and ambient air temperature on a summer design day.

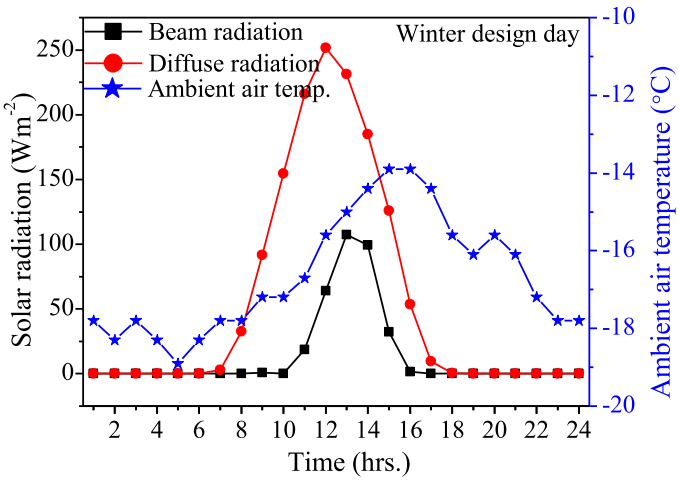

Fig. 3b. Hourly variation of the horizontal beam, diffuse solar irradiation, and ambient air temperature on a winter design day.

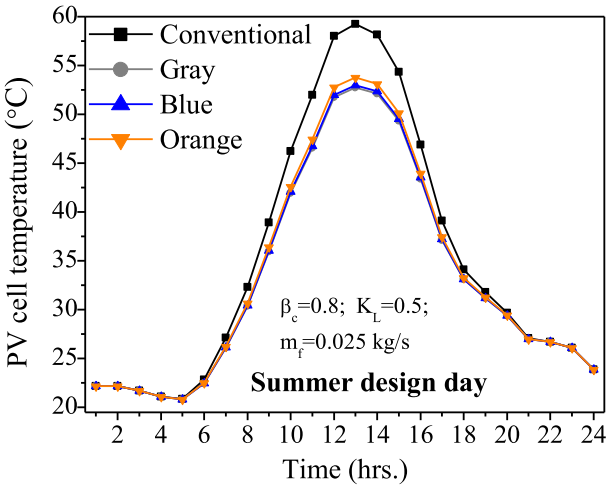

Fig. 4a. Hourly variation of PV cell temperature for different color PV modules integrated as façade of DSF for summer design day.

summer and winter design days in Montreal, Canada. On both design days, solar radiation and ambient air temperature rise throughout the morning, peak in the afternoon, and then decline towards the evening. During the summer design day, beam radiation is the predominant component of total solar radiation. Conversely, diffuse radiation constitutes most of the total solar radiation on the winter design day. This radiation data has been used to calculate the total radiation on tilted surfaces with different orientations using the Liu and Jordan model. The computed total radiation and ambient air temperature serve as climatic inputs in the mathematical model to assess the impact of orientations of the PV façade on the performance of the Double Skin Facade (DSF) system.

6.1. *Influence of PV color on the performance of DSF*

The temperature of PV cells in a conventional PV module with a clear front glass cover is compared to that in PV modules with grey, blue, and orange-colored front glass covers for a summer design day, as illustrated in Fig. 4a. These modules form the exterior façade of the considered DSF system. During sunshine hours, the PV cell temperature of the conventional PV module is higher than that of the colored PV modules due to the higher transmissivity of the clear front glass. The sputter coating

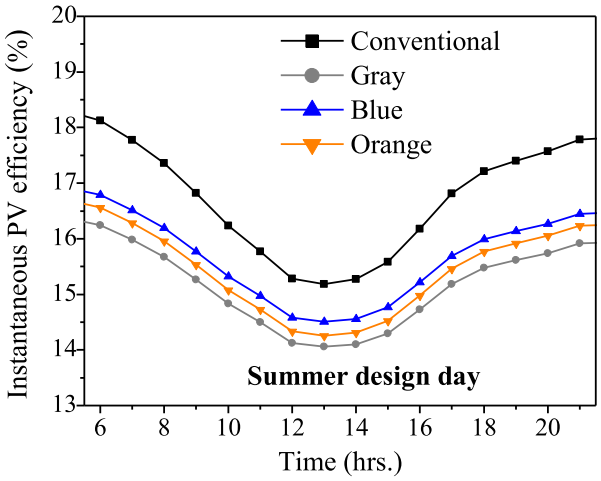

Fig. 5a. Hourly variation of instantaneous PV cell efficiency for different color PV modules integrated as façade of DSF for summer design day.

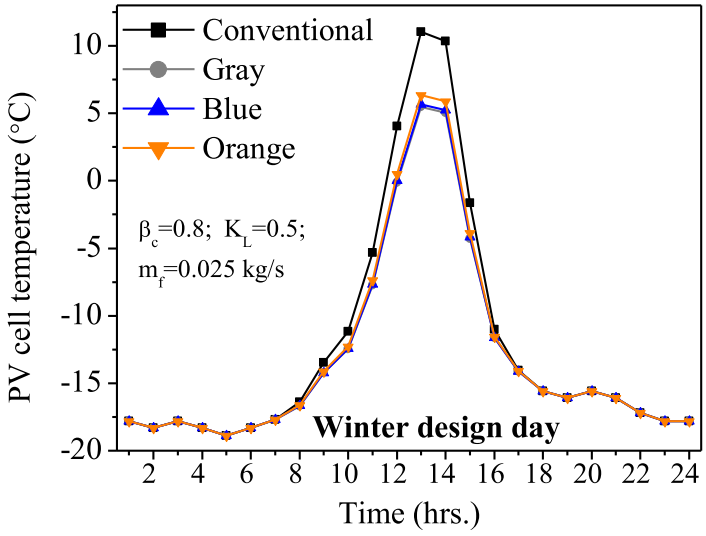

Fig. 4b. Hourly variation of PV cell temperature for different color PV modules integrated as façade of DSF for winter design day.

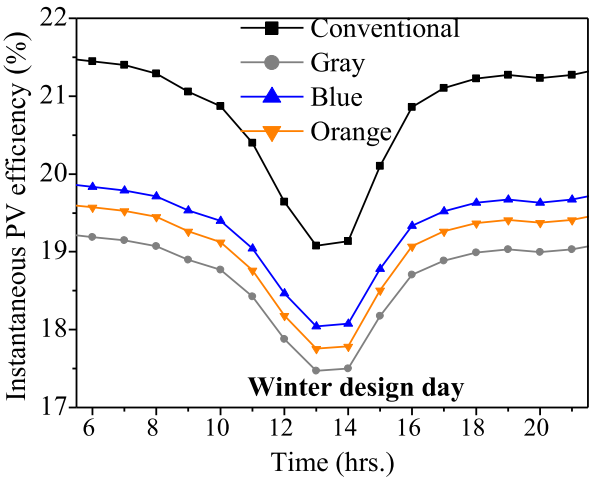

Fig. 5b. Hourly variation of PV cell efficiency for different color PV modules integrated as façade of DSF for winter design day.

layer used for coloration on the inner surface of the clear front glass reduces its transmissivity, thereby decreasing the amount of solar radiation reaching the PV cells and resulting in lower PV cell temperatures. Among the colored PV modules, the orange-colored PV module exhibits a slightly higher temperature than the blue and grey-colored PV modules, which show nearly identical PV cell temperatures. This is because the orange-colored PV module's transmissivity is higher than the blue and grey-colored PV modules. Notably, the temperature difference between the conventional and colored PV modules is most significant during peak sunshine hours. For instance, at 13:00 h, the PV cell temperature of the conventional PV module is 5.5 °C, 6.2 °C, and 6.5 °C higher than that of the orange, blue, and grey-colored PV modules, respectively. This behavior is consistent for the winter design day, as depicted in Fig. 4b, although the peak PV cell temperatures are significantly lower in winter due to reduced solar irradiation and lower ambient air temperatures. On this day at 13:00 h, the PV cell temperature of the conventional PV module is 4.7 °C, 5.4 °C, and 5.6 °C higher than that of the orange, blue, and gray-colored PV modules, respectively.

Fig. 5a and Fig. 5b illustrate the variation in instantaneous PV cell electrical efficiency for conventional and colored PV modules on summer and winter design days, respectively. As a thumb rule, the efficiency

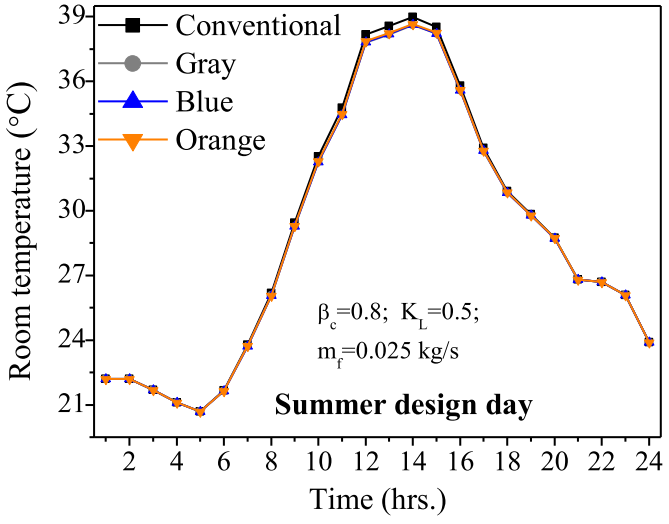

Fig. 6a. Hourly variation of average room air temperature for different color PV modules integrated as façade of DSF for summer design day.

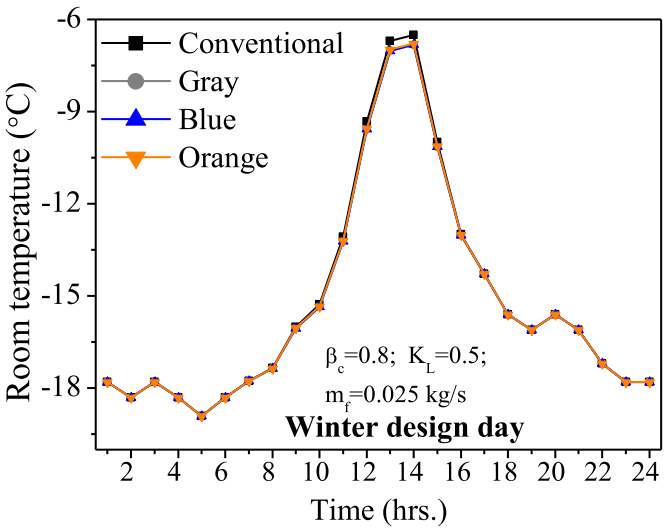

Fig. 6b. Hourly variation of average room air temperature for different color PV modules integrated as façade of DSF for winter design day.

varies inversely with PV cell temperature; hence, as PV cell temperature increases, efficiency decreases. However, this rule does not hold true considering color and conventional PV modules. Here, despite having a higher PV cell temperature, the conventional PV module exhibits higher efficiency because the STC efficiency of a conventional PV module is higher than the colored PV module. The difference in the efficiencies is notable during peak sunshine hours; for instance, at 13:00 h, the conventional PV module is 6.2 %, 4.4 %, and 7.5 % more efficient than orange, blue, and gray PV modules, respectively, for summer design day. For winter design days, the conventional module is 6.9 %, 5.4 %, and 8.5 % more efficient than orange, blue, and gray PV modules. Further, when compared among color PVs, the orange-colored PV module has a higher PV cell temperature than the gray PV module because of higher transmittance value and higher instantaneous PV efficiency, as the STC efficiency of gray PV is lower than orange PV. Hence, it is worth mentioning that instantaneous PV efficiency is decided by both the transmittance and STC efficiency.

Figs. 6a and 6b depict the hourly variation of air temperature inside a room equipped with a double skin façade system utilizing conventional PV modules with a clear front glass cover and colored front glass covers during summer and winter design days, respectively. The plots indicate that the impact of the colored front glass cover on room air temperature is minimal. However, during peak sunshine hours, the room temperature with the conventional clear glass PV module façade is slightly higher

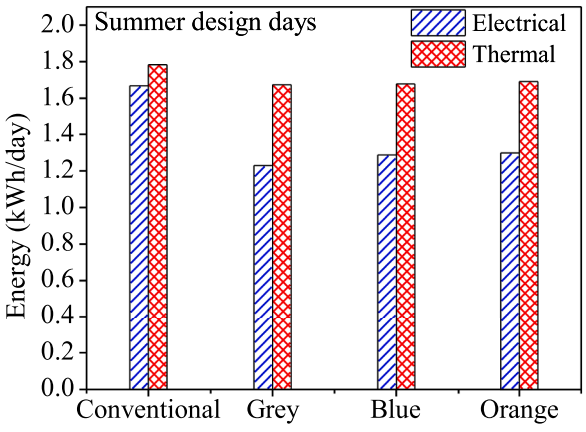

Fig. 7a. Daily electrical and thermal energy for different color PV modules integrated as façade of DSF for summer design day.

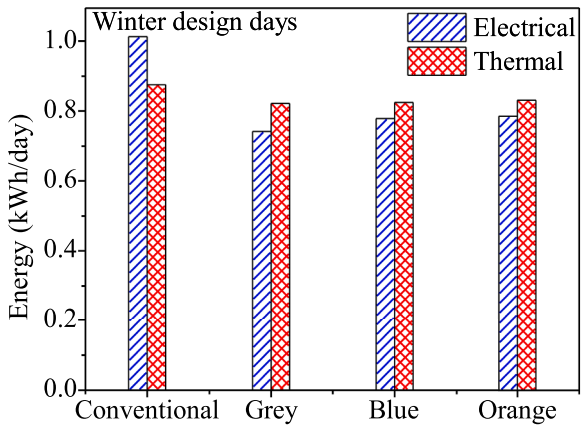

Fig. 7b. Daily electrical and thermal energy for different color PV modules integrated as façade of DSF for winter design day.

than that of rooms with colored PV façades. As anticipated, the average room air temperature on the summer design day is substantially higher than on the winter design day due to greater insolation and higher ambient air temperatures. To manage room air temperature effectively according to prevailing climatic conditions, strategies such as reducing the transmissivity of the interior glass façade, increasing the area of the exterior opaque PV façade, or reducing the transmissivity of the exterior glass façade can be employed.

Figs. 7a and 7b illustrate the daily electrical and thermal energy outputs of Double Skin Facade (DSF) systems incorporating conventional clear front glass PV modules and colored front glass PV modules for summer and winter design days, respectively. The DSF with conventional PV modules generates more electrical and thermal energy than the DSF with colored PV modules. This is attributed to the clear front glass PV's higher STC efficiency and transmissivity, allowing greater solar energy penetration to the PV cells. Although this results in higher PV temperatures and, consequently, higher thermal energy generation, it lowers the instantaneous efficiency of the PV cells. However, increased available solar radiation due to higher transmissivity compensates for the instantaneous efficiency reduction, leading to an overall enhancement in electrical energy generation. Among the colored PV modules, the gray PV module generates less electrical energy than the orange and blue PV modules due to its lower Standard Test Condition (STC) efficiency. However, all colored PV modules produce approximately the same amount of thermal energy. This behavior of DSF with conventional and colored PV remains consistent for the winter design day, as shown in Fig. 7b, although the energy outputs are significantly lower in winter due to reduced solar irradiation. Notably, the difference in thermal and electrical energies between the DSF with conventional PV modules and the DSF with colored PV modules is more pronounced in winter than in summer. This is due to the greater disparity in instantaneous PV cell efficiency caused by the cooler ambient temperatures during winter, as depicted in Fig. 5b.

6.2. *Influence of PV orientation on the performance of DSF*

Fig. 8a illustrates the effect of PV façade orientation on the peak PV cell and room air temperatures of a Double Skin Façade (DSF) system during a winter design day. A 0-degree orientation represents a south-facing PV DSF system, while +90° and −90° correspond to east and west-facing systems. Fig. 8a indicates that both PV cell and room air temperatures increase as the orientation angle shifts towards the west up to 30°, after which both temperatures decrease with further westward orientation. In contrast, as the PV DSF is oriented towards the east, both PV cell and room air temperatures decrease with increasing orientation angle, reaching their minimum values for the east-facing PV DSF. This behavior is primarily because of the asymmetric distribution of horizontal beam radiation and ambient air temperature around solar noon, with higher values occurring in the afternoon, as shown by Figs. 3a and 3b. The PV cell and room air temperatures for the south-facing DSF are 16 °C and 5.4 °C higher, respectively, compared to the east-facing DSF, and 3.1 °C and 2.4 °C higher, respectively, compared to the west-facing DSF. Similarly, Fig. 8b depicts the variation in PV cell and room air temperatures with different orientations of the PV DSF for a summer design day. Here, PV cell and room air temperatures increase when the PV DSF system is oriented towards the west (+90) from the south and decrease when oriented towards the east (−90) from the south. In this case, the PV cell and room air temperatures for the south-facing DSF are 10.1 °C and 6.2 °C higher, respectively, compared to the east-facing DSF, and 14.0 °C and 5.3 °C lower, respectively, compared to the west-facing DSF. Notably, the difference in PV cell and room air temperatures between the south-facing DSF and the west-facing DSFs is more pronounced in summer than in winter. This is because orientation-dependent beam radiation constitutes the dominant component of total radiation on a summer design day, whereas orientation-independent diffuse radiation dominates the total radiation on a winter design day.

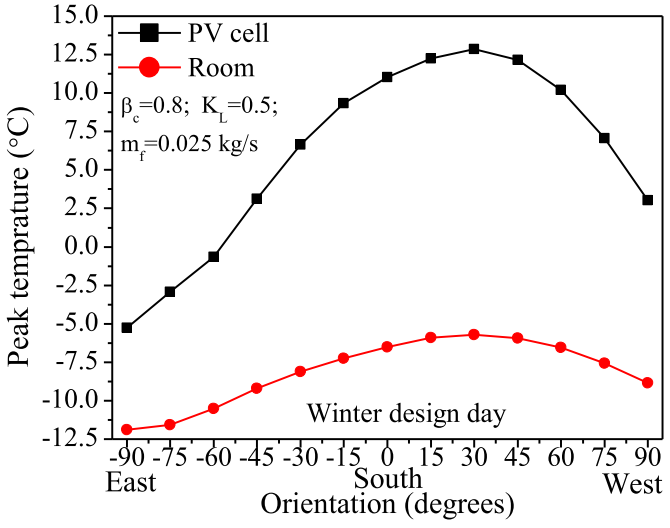

Fig. 8a. Peak PV cell and room air temperatures for different orientations of PV DSF for winter design day.

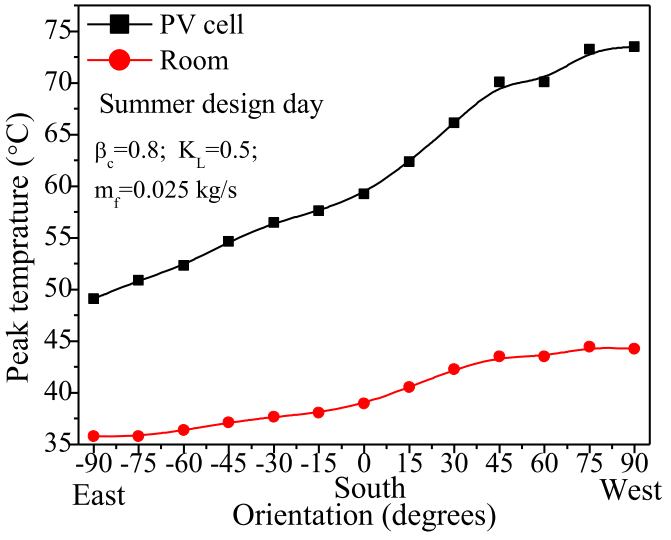

Fig. 8b. Peak PV cell and room air temperatures for different orientations of PV DSF for summer design day.

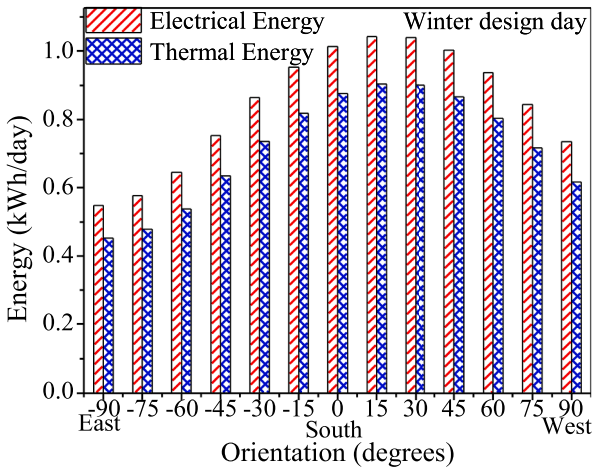

Fig. 9a. Daily electrical and thermal energies for different orientations of PV DSF for winter design day.

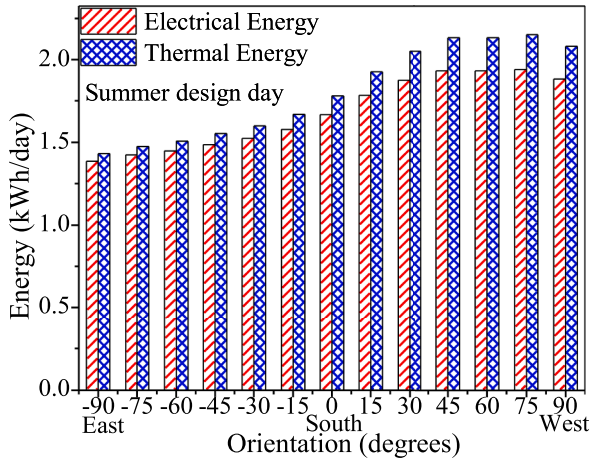

Fig. 9b. Daily electrical and thermal energies for different orientations of PV DSF for summer design day.

The variation of electrical and thermal energy for different orientations of the DSF system is presented in Fig. 9a for a winter design day. Here, both the electrical and thermal energy increase with an increase in orientation angle up to 30° towards the west as measured from the south, and with further increase in orientation angle, the energies decrease. However, the thermal and electrical energy gradually reduces when orientation changes towards the east from the south. Compared to a south-facing DSF, an east-facing DSF generates 466 Wh less electrical energy and 423 Wh lesser thermal energy daily. At the same time, a west-facing DSF produces 278 Wh less electrical energy and 258 Wh less thermal energy daily. Similarly, the variation of electrical and thermal energy for different orientations of the DSF system is presented in Fig. 9b for a summer design day. On this day, the values of electrical and thermal energies reduce with an increase in orientation angle towards the east as measured from the south, whereas an increase in both energies is observed when the orientation is changed towards the west. Compared to a south-facing DSF, an east-facing DSF generates 282 Wh less electrical energy and 350 Wh less thermal energy daily. Conversely, a west-facing DSF produces 218 Wh more electrical energy and 300 Wh more thermal energy daily.

7. Conclusions

In this study, the performance of Double Skin Facade (DSF) systems integrated with conventional and colored (orange, blue, and gray) photovoltaic modules with different orientations has been comprehensively analyzed for the climatic conditions of Montreal, Canada. These PV modules have been integrated as the exterior façade of a DSF system. The investigation evaluated the PV cell temperature, electrical efficiency, room air temperature, and energy outputs of the PV DSF system for summer and winter design days. The following are the key conclusions of the detailed study:

- In a DSF system, the conventional photovoltaic (PV) module with clear front glass exhibited higher PV cell temperatures than colored PV modules due to its greater transmissivity, with temperature differences peaking at 13:00 h by 5.5 °C, 6.2 °C, and 6.5 °C for orange, blue, and gray PV modules, respectively. Despite higher temperatures, the clear glass PV modules showed superior instantaneous efficiency due to their higher Standard Test Condition (STC) efficiency. This indicates that the inverse relationship between PV cell efficiency and temperature does not apply when comparing conventional and colored PV modules with different STC efficiencies.
- The room air temperature in spaces equipped with a PV-DSF system, using conventional PV modules with clear or colored front glass, is approximately the same. This implies that colored front glass covers in PV modules have an insignificant impact on room air temperature.
- DSF systems equipped with conventional clear front glass PV modules exhibit superior daily electrical and thermal energy outputs compared to those with colored PV modules. This advantage is attributed to their higher STC efficiency and transmissivity, which improve solar energy absorption. The electrical energy yield of DSF systems with Gray, Blue, and Orange colored PV modules is 26.0 %, 22.7 %, and 22.13 % lower than that of conventional clear glass PV modules. Similarly, the thermal energy yield for DSF systems with Gray, Blue, and Orange colored PV modules is reduced by 6.0 %, 5.8 %, and 5.0 % compared to conventional clear glass PV modules.
- Orientation significantly influences peak PV cell and room air temperatures and electrical and thermal energy generation in DSF systems. During a winter design day, south-facing orientations exhibit higher temperatures compared to east and west-facing orientations. However, west-facing DSFs show significantly higher peak PV cell temperature, room air temperature, and electrical and thermal energy than south-facing ones on a summer design day. A west-facing DSF produces 218 Wh more electrical energy and 300 Wh more thermal energy daily. This indicates that south-facing is not always the optimal orientation, and the value of optimal orientation depends on the hourly distribution of the beam, diffuse solar irradiation, and ambient air temperature. When solar irradiation is skewed towards the afternoon hours, west-facing DSFs yield higher electrical and thermal energy, and for the distribution skewed toward forenoon hours, an east-facing DSF will yield higher energies.

In conclusion, the mathematical model developed in this study offers a practical tool for planning PV double-skin facades in heritage buildings, addressing the unique constraints of color and orientation. The model ensures that heritage buildings can integrate modern renewable energy solutions without compromising their historical and aesthetic integrity by enabling the assessment of PV with different colors and orientations.

8. Limitations and future prospects

The model developed in this study is well-suited for the preliminary design and analysis of ventilated PV DSF systems but has certain limitations due to simplifying assumptions. Notably, the model excludes internal heat gains from lighting, occupants, and appliances and assumes laminar flow within the cavity. It also only considers cavity airflow in one direction, specifically supply air, without accounting for the possibility of other airflow modes, such as exhaust air for cooling and

external and internal air curtains. The present study did also not explore the impact of complex façade geometries that could enhance solar exposure and influence DSF performance.

Future work could address these limitations by incorporating internal heat gains, considering turbulent flow conditions within the cavity, and expanding the model to include different airflow modes. Additionally, exploring the impact of more complex geometries on system performance would provide a more comprehensive understanding. Further investigation should also evaluate the economic and environmental feasibility of the system, focusing on key indicators like Return on Investment (ROI) and other financial and environmental metrics. This would offer valuable insights for stakeholders considering the adoption of PV DSF systems, ensuring both technical viability and economic attractiveness.

CRediT authorship contribution statement

Somil Yadav: Methodology, Investigation, Formal analysis, Conceptualization. **Caroline-Hachem Vermette:** . **Md.Nadim Heyat Jilani:** Writing – original draft, Investigation. **Gilles Desthieux:** Writing – review & editing, Conceptualization.

Declaration of competing interest

The authors certify that they have NO affiliations with or involvement in any organization or entity with any financial interest (such as honoraria; educational grants; participation in speakers' bureaus; membership, employment, consultancies, stock ownership, or other equity interest; and expert testimony or patent-licensing arrangements), or non-financial interest (such as personal or professional relationships, affiliations, knowledge or beliefs) in the subject matter or materials discussed in this manuscript.

Appendix A

The energy balance for the air flowing through the cavity having a cross-section ($b \times dx$) on the rear of the PV façade is written below.

$$h_{bs,f}\left(T_{bs}-T_{fpv}\right)bdx = \dot{m}_f C_f \frac{dT_{fpv}}{dx}dx + U_{f,r}\left(T_{fpv}-T_r\right)bdx \tag{A1}$$

Substituting the expression of 'T_{bs}' in the above equation from Eq. (6c) and rearranging the Eq. (A.1) as below.

$$\frac{dT_{fpv}}{dx} = -pT_{fpv} + q \tag{A2}$$

where

$$p = \frac{\left(U_{f,r}+h_{bs,f}\right)b}{\dot{m}_f C_f};\; q = \frac{\left(T_r U_{f,r} + U_{ta}T_{am} + h_{p2}h_{p1}\alpha_{eff}I_{glob,inc}\right)b}{\dot{m}_f C_f} \tag{A3}$$

The above ordinary differential equation can be solved for 'T_{fpv}' using the boundary conditions, i.e., at $x = 0,\; T_{fpv} = T_{fpv,in}$.

$$T_{fpv} = \frac{q}{p}\left(1-e^{-px}\right) + T_{fpv,in}e^{-px} \tag{A4}$$

$$T_{fpv} = \left(\frac{U_{f,r}T_r + U_{ta}T_{am} + h_{p2}h_{p1}\alpha_{eff}I_{glob,inc}}{U_L}\right)\left(1-e^{-px}\right) + T_{fpv,in}e^{-px} \tag{A5}$$

The air temperature at the outlet of the duct can be as below.

$$T_{fpv,out} = T_{fpv}\left(x = L_{pv}\right) = \left(\frac{U_{f,r}T_r + U_{ta}T_{am} + h_{p2}h_{p1}\alpha_{eff}I_{glob,inc}}{U_L}\right)\left(1-e^{-pL_{pv}}\right) + T_{fpv,in}e^{-pL_{pv}} \tag{A6}$$

The average air temperature over the duct length 'L' can be determined as follows.

$$\overline{T}_{fpv} = \frac{1}{L_{pv}}\int_0^{L_{pv}} T_{fpv}dx \tag{A7}$$

After substituting the expression 'T_{fpv}' in the above equation, '$\overline{T}_{fpv}$' is computed as below. This average air temperature will be used to compute heat transfer coefficients.

$$\overline{T}_{fpv} = \left(\frac{U_{f,r}T_r + U_{ta}T_{am} + h_{p2}h_{p1}\alpha_{eff}I_{glob,inc}}{U_L}\right)\left(1-\frac{1-e^{-pL_{pv}}}{pL_{pv}}\right) + T_{fpv,in}\left(\frac{1-e^{-pL_{pv}}}{pL_{pv}}\right) \tag{A8}$$

where

$$h_{p2} = \frac{h_{bs,f}}{U_{tT}+h_{bs,f}};\; U_{ta} = \frac{h_{bs,f}U_{tT}}{U_{tT}+h_{bs,f}};\; U_L = \left(U_{ta}+U_{f,r}\right);\; U_{f,r} = \left[\frac{D_i}{K_i}+\frac{1}{h_r}\right]^{-1};\; p = \frac{bU_L}{\dot{m}_f C_f} \tag{A9}$$

References

[1] O. Iken, M. Dlimi, R. Agounoun, I. Kadiri, A. Zoubir, K. Sbai, Numerical investigation of energy performance and cost analysis of Moroccan's building smart walls integrating vanadium dioxide, Sol. Energy 179 (2019) 249–263.

[2] D. D'Agostino, D. Parker, I. Epifani, D. Crawley, L. Lawrie, How will future climate impact the design and performance of nearly zero energy buildings (NZEBs)? Energy 240 (2022) 122479.

[3] H. Yazdani, M. Baneshi, Building energy comparison for dynamic cool roofs and green roofs under various climates, Sol. Energy 230 (2021) 764–778.

[4] M. Perino, V. Serra, Switching from static to adaptable and dynamic building envelopes: a paradigm shift for the energy efficiency in buildings, J. Facade Des. Eng. 3 (2015) 143–163.

[5] M.K. Sharma, S. Preet, J. Mathur, A. Chowdhury, S. Mathur, Parametric analysis of factors affecting thermal performance of photovoltaic triple skin façade system (PV-TSF), J. Build. Eng. 40 (2021) 102344, https://doi.org/10.1016/j.jobe.2021.102344.

[6] U. Berardi, T. Wang, Daylighting in an atrium-type high performance house, Build. Environ. 76 (2014) 92–104, https://doi.org/10.1016/j.buildenv.2014.02.008.

[7] E. Gratia, A. De Herde, Guidelines for improving natural daytime ventilation in an office building with a double-skin facade, Sol. Energy 81 (2007) 435–448.

[8] S. Preet, J. Mathur, S. Mathur, Influence of geometric design parameters of double skin façade on its thermal and fluid dynamics behavior: a comprehensive review, Sol. Energy 236 (2022) 249–279, https://doi.org/10.1016/j.solener.2022.02.055.

[9] M. Torres, P. Alavedra, A. Guzmán, E. Cuerva, C. Planas, R. Clemente, V. Escalona, Double skin façades–cavity and exterior openings dimensions for saving energy on mediterranean climate, (2007).

[10] N. Ziasistani, F. Fazelpour, Comparative study of DSF, PV-DSF and PV-DSF/PCM building energy performance considering multiple parameters, Sol. Energy 187 (2019) 115–128.

[11] C. Marinosci, P.A. Strachan, G. Semprini, G.L. Morini, Empirical validation and modelling of a naturally ventilated rainscreen façade building, Energy Build. 43 (2011) 853–863.

[12] S. Fantucci, C. Marinosci, V. Serra, C. Carbonaro, Thermal performance assessment of an opaque ventilated façade in the summer period: calibration of a simulation model through in-field measurements, Energy Procedia 111 (2017) 619–628.

[13] N.M. Mateus, A. Pinto, G.C. Da Graça, Validation of EnergyPlus thermal simulation of a double skin naturally and mechanically ventilated test cell, Energy Build. 75 (2014) 511–522.

[14] A.M. Qahtan, Thermal performance of a double-skin façade exposed to direct solar radiation in the tropical climate of Malaysia: a case study, Case Stud. Thermal Eng. 14 (2019) 100419.

[15] A. De Gracia, A. Castell, L. Navarro, E. Oró, L.F. Cabeza, Numerical modelling of ventilated facades: a review, Renew. Sustain. Energy Rev. 22 (2013) 539–549, https://doi.org/10.1016/j.rser.2013.02.029.

[16] Z.J. Zhai, Q.Y. Chen, Performance of coupled building energy and CFD simulations, Energy Build. 37 (2005) 333–344.

[17] J. Srebric, Q. Chen, L. Glicksman, A coupled airflow and energy simulation program for indoor thermal environmental studies, (2000). https://www.osti.gov/biblio/20104808 (accessed July 10, 2023).

[18] C. Tzikas, R.M.E. Valckenborg, M. Dörenkämper, M.N. van den Donker, D. D. Lozano, Á. Bognár, R. Loonen, J.L.M. Hensen, W. Folkerts, Outdoor characterization of colored and textured prototype PV facade elements, in: Proceedings of the 35th European Photovoltaic Solar Energy Conference and Exhibition, 2018, pp. 1468–1471.

[19] N. Jolissaint, R. Hanbali, J.-C. Hadorn, A. Schüler, Colored solar façades for buildings, Energy Procedia 122 (2017) 175–180.

[20] H. Lee, R. Lee, D. Kim, J. Yoon, H. Kim, G. Lee, Performance evaluation of sputter-coating based color BIPV modules under the outdoor operational condition: a comparative analysis with a non-color BIPV module, Energy Rep. 8 (2022) 5580–5590, https://doi.org/10.1016/j.egyr.2022.04.034.

[21] S. Yadav, C. Hachem-Vermette, Comprehensive assessment of double skin façades: a mathematical model for evaluating influence of KL ratio on electrical and thermal performances, and indoor conditions, Energy Build. 303 (2024) 113762, https://doi.org/10.1016/J.ENBUILD.2023.113762.

[22] B.Y.H. Liu, R.C. Jordan, The interrelationship and characteristic distribution of direct, diffuse and total solar radiation, Sol. Energy 4 (1960) 1–19, https://doi.org/10.1016/0038-092X(60)90062-1.

[23] M. Kacira, M. Simsek, Y. Babur, S. Demirkol, Determining optimum tilt angles and orientations of photovoltaic panels in Sanliurfa, Turkey, Renew. Energy 29 (2004) 1265–1275, https://doi.org/10.1016/j.renene.2003.12.014.

[24] G.N. Tiwari, A. Tiwari, Handbook of Solar Energy, Springer, 2016.

[25] D.L. Evans, Simplified method for predicting photovoltaic array output, Sol. Energy 27 (1981) 555–560, https://doi.org/10.1016/0038-092X(81)90051-7.

[26] Climate.OneBuilding.Org, 2024. https://climate.onebuilding.org/ (accessed August 12, 2024).

[27] B.Y.H. Liu, R.C. Jordan, The interrelationship and characteristic distribution of direct, diffuse and total solar radiation, Sol. Energy 4 (1960) 1–19, https://doi.org/10.1016/0038-092X(60)90062-1.

[28] A. Tiwari, M.S. Sodha, Parametric study of various configurations of hybrid PV/thermal air collector: experimental validation of theoretical model, Sol. Energy Mater. Sol. Cells 91 (2007) 17–28, https://doi.org/10.1016/J.SOLMAT.2006.06.061.